Finite element analysis of transient natural convection in an odd-shaped enclosure

P. Nithiarasu, T. Sundararajan and K.N. Seetharamu

Department of Mechanical Engineering, Indian Institute of Technology, Madras, India

Received April 1995
Revised July 1996
Accepted July 1997

Nomenclature

See Table 1a.

AR = aspect ratio
g = acceleration due to gravity
h = heat transfer coefficient
H = height
k = thermal conductivity
L = length
N = shape function
$\underline{Nu}$ = local Nusselt number
$\overline{Nu}$ = average Nusselt number = $h L_{ref}/k$
p = pressure
Pr = Prandtl number = ν/α
Ra = Rayleigh number = $g \beta \Delta T L^3_{ref}/\alpha \nu$
T = temperature
u,v = velocities in x and y directions

Greek symbols

α = thermal diffusivity
β = coefficient of thermal expansion
ν = kinematic viscosity
ρ = density
τ = time
ψ = stream function

Subscripts

D = lumped matrix
i = initial, ith node
j,k = jth and kth nodes
max = maximum
ref = reference

Superscripts

n = time level

Table 1a.

Introduction

A study of transient natural convective flow and heat transfer in an odd-shaped geometry is presented here. The geometry considered is a combination of the horizontal and vertical enclosure shapes. Most of the available literature on this topic concerns regular geometries such as rectangular enclosures and cylindrical annuli (de Vahl Davis, 1983; Elder, 1965; Fu and Jou, 1991; Fu *et al.*, 1989; Ostrach, 1988; Satya Sai *et al.*, 1993; Scozia and Frederick, 1991; Tabarrok and Lin, 1977; Yeung, 1989; Yin *et al.*, 1978), while actual applications demand the consideration of irregular shapes. In particular, for applications involving the cooling of electronic equipment, solar collectors, ingot castings, thermal hydraulic analysis of LMFBR etc., it is often necessary to consider geometries such as the present one (Aung, 1991; Betts *et al.*, 1983; Vafai and Ettefagh, 1990).

Only a few studies have so far been reported which take into account the irregularities in geometry. For instance, Evren-Selamet *et al.* (1992) studied natural convection in a slot having the shape of a bottle. General irregular geometries with differentially heated walls have been dealt with by Coulter and

International Journal of Numerical Methods for Heat & Fluid Flow
Vol. 8 No. 2, 1998, pp. 199–216.

Guceri (1987). Campo *et al.* (1988) have analysed the natural convection in a triangular enclosure using the Galerkin finite element method with stream function – vorticity – temperature formulation.

Heat transfer between an inner body and the surrounding enclosure is another important area which has received attention in recent years. Warrington and Powe (1985) have experimentally analysed the natural convection between concentrically located isothermal inner bodies of spherical, cylindrical and cubical geometry and their cubical enclosures. The paper concludes that the enclosure dimensions have a more significant effect on temperature profile and heat transfer than the enclosure shape. Garg (1992) investigated the natural convection heat transfer between concentric spheres using the finite difference method. Arbitrary shaped inner bodies within an enclosure have been considered by Glakpe and Asfaw (1991).

A majority of the existing studies on two dimensional rectangular enclosures have considered only vertical or horizontal orientation of the cavity. In the present study, the flow and heat transfer phenomena in a vertical enclosure with a horizontal extension are analysed for various types of boundary conditions. A detailed parametric study has been carried out to analyse the effects of geometry, Rayleigh number and the nature of the prescribed boundary conditions.

Problem definition and formulation

Natural convection in air, in the space between a hot inner body and its enclosure, is considered (Figure 1 (a)). The air inside the enclosure is initially at a uniform temperature T_i and is motionless. From this condition the inner wall temperature is suddenly raised to T_h and held constant thereafter. The outer wall temperature is maintained at the initial value T_i while the other two sides are insulated. The transient phenomena that follow the sudden imposition of the inner wall boundary condition are studied. Apart from the main problem defined here, a few variants with respect to the specification of boundary conditions have also been considered.

After invoking the Boussinesq approximation, the non-dimensional governing equations for two dimensional laminar flow and heat transfer are given by:

Continuity equation

$$\frac{\partial u}{\partial x} + \frac{\partial v}{\partial y} = 0.0 \tag{1}$$

x – momentum equation

$$\frac{\partial u}{\partial \tau} + u\frac{\partial u}{\partial x} + v\frac{\partial u}{\partial y} = -\frac{\partial p}{\partial x} + Pr\left(\frac{\partial^2 u}{\partial x^2} + \frac{\partial^2 u}{\partial y^2}\right) \tag{2}$$

(a)

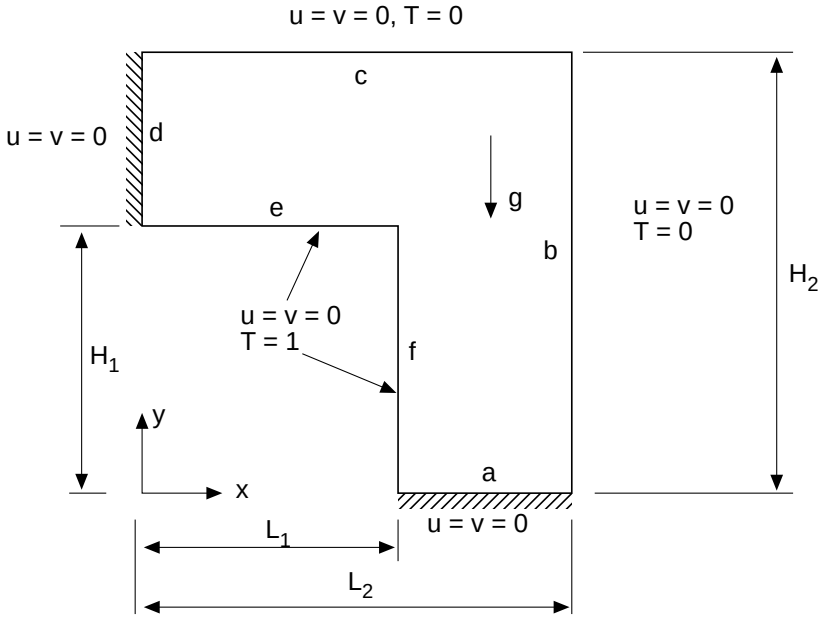

(b)

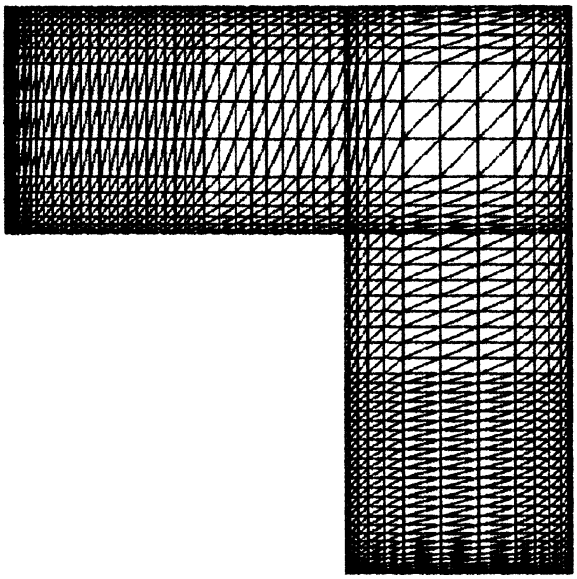

Figure 1.
(a) geometry of the problem; (b) finite element mesh

y – momentum equation

$$\frac{\partial v}{\partial \tau} + u\frac{\partial v}{\partial x} + v\frac{\partial v}{\partial y} = -\frac{\partial p}{\partial y} + Pr\left(\frac{\partial^2 v}{\partial x^2} + \frac{\partial^2 v}{\partial y^2}\right) + RaPrT \tag{3}$$

energy equation

$$\frac{\partial T}{\partial \tau} + u\frac{\partial T}{\partial x} + v\frac{\partial T}{\partial y} = \frac{\partial^2 T}{\partial x^2} + \frac{\partial^2 T}{\partial y^2} \tag{4}$$

The scaling employed for the non-dimensional variables are:

$$x = \frac{\overline{x}}{L_{ref}},\ y = \frac{\overline{y}}{L_{ref}},\ u = \frac{\overline{u}L_{ref}}{\alpha},\ v = \frac{\overline{v}L_{ref}}{\alpha}$$
$$\tau = \frac{\overline{\tau}\alpha}{L_{ref}^2},\ p = \frac{\overline{p}L_{ref}^2}{\rho\alpha^2},\ T = \frac{\overline{T} - \overline{T}_i}{\overline{T}_h - \overline{T}_i} \tag{5}$$

where L_{ref} is the characteristic dimension and in the present study it is the height of the cavity.

In the above expressions the over-bar denotes a dimensional variable. The boundary and initial conditions for the problem are (Figure 1(a)):

u = v = 0	on the surfaces a,b,c,d,e and f
T = 0	on b and c
T = 1	on e and f
$\frac{\partial T}{\partial n} = 0$	on a and d
u = v = T = 0	at $\tau = 0$

The non-dimensional parameters which have been varied in the study are the width ratio (WR) and Rayleigh number (Ra). In order to investigate the effects of boundary conditions, a problem with the following boundary condition is considered.

u = v = 0	on the surfaces a,b,c,d,e and f
T = 0	on d
T = 1	on a
$\frac{\partial T}{\partial n} = 0$	on b,c,e and f
u = v = T = 0	at $\tau = 0$

Solution procedure

The Galerkin finite element method using primitive variables of u, v, p and T has been employed. For updating the pressure field with respect to time, the continuity equation is converted into a Poisson equation for pressure through the Eulerian velocity correction procedure (Nithiarasu *et al.*, 1995; Ramaswamy, 1988; Ramaswamy *et al.*, 1992). The cavity geometry is discretized to form a numerical mesh, with the help of three node triangular elements. The velocity, pressure and temperature variables within each element are expressed as

$$\begin{aligned} u &= N_i u_i + N_j u_j + N_k u_k, \quad & v &= N_i v_i + N_j v_j + N_k v_k \\ T &= N_i T_i + N_j T_j + N_k T_k, \quad & p &= N_i p_i + N_j p_j + N_k p_k \end{aligned} \tag{6}$$

where N_i, N_j and N_k are the shape functions. The advection terms in each of the governing equations have been discretized by the Adams Bashforth method while diffusion terms have been handled using the Euler implicit scheme (Nithiarasu *et al.*, 1995; Ramaswamy, 1988; Ramaswamy *et al.*, 1992). The various steps employed for each time increment, in the semi-implicit scheme applied to the weighted residual form of governing equations, are given below.

Step 1

Calculation of fictitious velocities from momentum equations without pressure terms:

$$[M + K^u]\,\tilde{u} = [M]u^n + \Delta\tau^n \left(F^u - [A1]u^n - [A2]u^{n-1}\right) \tag{7}$$

$$[M + K^v]\,\tilde{v} = [M]v^n + \Delta\tau^n \left(F^v - [A1]v^n - [A2]v^{n-1} + GT^n\right) \tag{8}$$

Step 2

Calculation of pressure from pressure Poisson equation:

$$[K^p]p^{n+1} = F^p \tag{9}$$

Step 3

Velocity correction:

$$[M_D]u^{n+1} = [M_D]\tilde{u} + \Delta\tau^n R^u \tag{10}$$

$$[M_D]v^{n+1} = [M_D]\tilde{v} + \Delta\tau^n R^v \tag{11}$$

Step 4

Solution of energy equation:

$$[M + K^T]T^{n+1} = [M]T^n + \Delta\tau^n(F^T - [A1]T^n - [A2]T^{n-1}) \tag{12}$$

The entries of the matrices and vectors in the above equations are defined as

$$M_{ij} = \int N_i N_j d\Omega \tag{13}$$

$$A1_{ij} = \frac{3}{2}\int N_i \left[(N_k u_k^n)\frac{\partial N_j}{\partial x} + (N_k v_k^n)\frac{\partial N_j}{\partial y}\right] d\Omega \tag{14}$$

$$A2_{ij} = -\frac{1}{2}\int N_i \left[(N_k u_k^{n-1})\frac{\partial N_j}{\partial x} + (N_k v_k^{n-1})\frac{\partial N_j}{\partial y}\right] d\Omega \tag{15}$$

$$K_{ij}^p = \int \left[\frac{\partial N_i}{\partial x}\frac{\partial N_j}{\partial x} + \frac{\partial N_i}{\partial y}\frac{\partial N_j}{\partial y}\right] d\Omega \tag{16}$$

$$K_{ij}^T = K_{ij}^p, \quad K_{ij}^v = PrK_{ij}^p, \quad K_{ij}^u = K_{ij}^v \tag{17}$$

$$G_{ij} = RaPrM_{ij} \tag{18}$$

$$F_i^u = \int N_i \frac{\partial u}{\partial n} d\Gamma, \quad F_i^v = \int N_i \frac{\partial v}{\partial n} d\Gamma \tag{19}$$

$$F_i^p = \int N_i \frac{\partial p}{\partial n} d\Gamma - \frac{1}{\Delta\tau^n}\int N_i \left[(\frac{\partial N_k}{\partial x}\tilde{u}_k) + (\frac{\partial N_k}{\partial y}\tilde{v}_k)\right] d\Omega \tag{20}$$

$$F_i^T = \int N_i \frac{\partial T}{\partial n} d\Gamma \tag{21}$$

$$R_i^u = \int N_i \frac{\partial N_k}{\partial x} p_k^{n+1} d\Omega, \quad R_i^v = \int \frac{\partial N_k}{\partial y} p_k^{n+1} d\Omega \tag{22}$$

The time marching is continued until the nodal velocities, pressure and temperature approach steady state within a specified difference in the value of the variable between two successive time steps. The tolerance value has been set as 10^{-7} for velocities and temperature, while it is 10^{-4} for pressure. The dimensionless time steps have been selected in the range of 10^{-3} to 10^{-6}, where lower values are employed for high Ra and vice versa.

Results and discussion

In order to validate the numerical scheme employed here, results have been predicted and compared against the benchmark results available in the literature for natural convection in a square cavity. The boundary conditions considered for the validation problem are those of differentially heated vertical walls and insulated horizontal walls. The Nusselt number values for different grid sizes are compared in Table I. This shows that the grid size of 41×41 is quite adequate for carrying out the calculations. The comparison of present

results with those available in literature (de Vahl Davis, 1983), are given in Table II. The Ra range considered for the comparison is 10^4 to 10^6.

It is observed from the table that all quantities predicted (average Nusselt number on the hot wall, $\overline{Nu}$, maximum stream function $|\psi_{max}|$, maximum vertical velocity v_{max}, and the maximum Nusselt number Nu_{max}) are in good agreement with the values in the literature. Minor differences observed in the two sets of results may be attributed to the different choices of element shapes and solution procedures. The numerical results of the reference paper cited here have been obtained by the finite difference technique using rectangular mesh, while triangular elements and the finite element solution procedure have been employed in the present study.

After validating the numerical scheme, it was felt necessary to perform a grid sensitivity analysis for the odd-shaped geometry considered. In order to select a suitable numerical grid, results at a Rayleigh number of 10^6 have been predicted using four different grids. Comparisons between the results obtained for these three grids are given in Table III.

It is evident from the table that grid 3 with 1,440 nodes is quite adequate for the problem considered. Therefore, grid 3 with non-uniform triangular elements (Figure 1(b)) has been employed for all numerical predictions of the present study.

Grid size	11×11	31×31	41×41
Average Nu	11.220	8.815	8.800

Table I. Average Nusselt number values along the hot wall of square cavity, Ra = 10^6

	Ra = 10^4		Ra = 10^5		Ra = 10^6	
Parameters	Present	de Vahl Davies (1983)	Present	de Vahl Davies (1983)	Present	de Vahl Davies (1983)
$\overline{Nu}$	2.245	2.238	4.521	4.509	8.800	8.817
$\lvert\psi_{max}\rvert$	5.179	5.071	9.800	9.612	17.200	16.750
v_{max}	19.816	19.617	68.860	68.590	222.460	219.360
Nu_{max}	3.518	3.528	7.859	7.717	17.400	17.925

Table II. Comparison of present results with benchmark solution (de Vahl Davis, 1983) on 41×41 non-uniform grid

	Number of nodes			
Parameters	800 (grid 1)	1,056 (grid 2)	1,440 (grid 3)	1,802 (grid 4)
$\overline{Nu}$	11.41	11.42	11.37	11.38
v_{max}	262.45	248.01	248.29	248.33
$\lvert\psi_{max}\rvert$	21.29	20.10	20.12	20.12

Table III. Grid selection for Ra = 10^6, WR = 0.3

Flow and isothermal patterns

The stream line and isothermal patterns for different Rayleigh numbers and Width ratios are shown in Figures 2, 3 and 4. These figures indicate a mixed flow structure between that of a vertical and a horizontal enclosure. The effects of such vortex flows upon the shapes of isotherms and wall heat transfer are also illustrated. In all the cases, stream function is calculated by solving the following vorticity equation.

$$\Delta^2 \psi = \frac{\partial u}{\partial y} - \frac{\partial v}{\partial x} \tag{23}$$

In Figure 2 it is seen that the vertical vortex is predominant and it fills a significant part of the horizontal extension also. The penetration of the vertical vortex into the horizontal chamber is more, for smaller WR. A small recirculatory vortex is observed at the bottom corner adjacent to the hot wall. The size of this vortex increases as WR is reduced. As regards the isotherms, these are almost parallel to isothermal walls indicating the predominance of heat conduction at a low Ra of 10^3. It is noted that at the vertex of the inner body, a high flux region develops owing to the clustering of stream lines as well as isotherms.

For a Rayleigh number of 10^5 (Figure 3), it is observed that the flow pattern in the horizontal part also exerts a significant influence, especially for larger

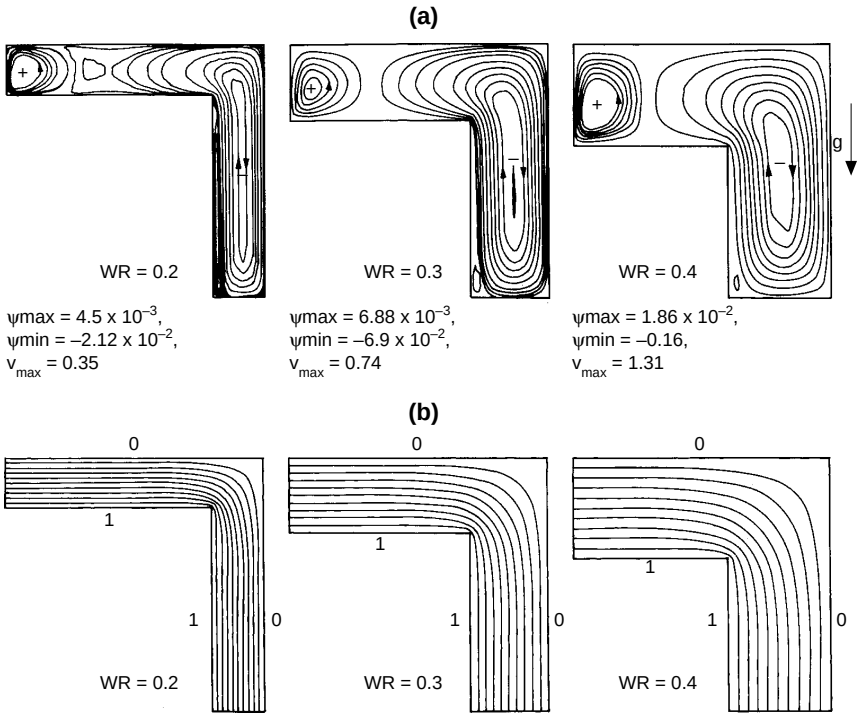

Figure 2.
Stream line (a) and isothermal (b) patterns for Ra = 10^3

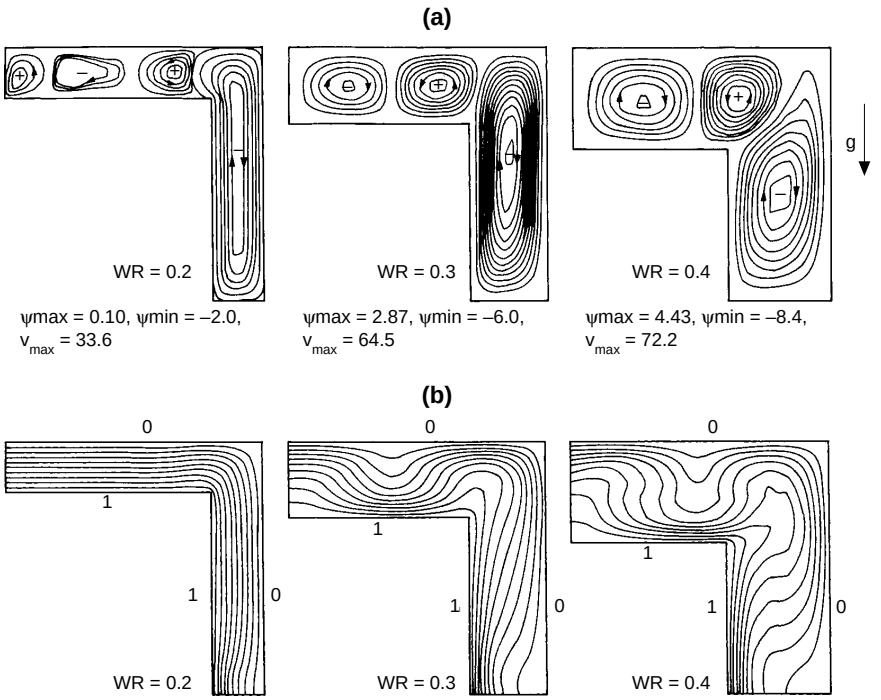

Figure 3.
Stream line (a) and isothermal (b) patterns for Ra = 10^5

width ratios. With lower width ratios, the vertical flow is still able to enter partly into the horizontal portion. Within the horizontal extension, the typical cellular convection pattern is observed. The number of cells within unit length, however, tends to increase for smaller WR. The isothermal patterns indicate that conduction is predominant for lower width ratios, while convection effects are significant at high width ratios. When convective effects are important alternate spots of high and low flux are observed.

The features seen at Ra = 10^5 are further accentuated for the Rayleigh number of 10^6 (Figure 4). The cellular pattern of the horizontal part becomes predominant for low WR. As regards the isotherms, it is seen that convective effects are significant for all WR values considered. The alternate spots of high and low heat fluxes are observed more clearly, especially in the horizontal part.

Figure 5 shows the stream line and isothermal patterns for different L_2/H_2 ratios at Ra = 10^6. For the two different ratios considered, the patterns are entirely different. In both the cases only two vortices are observed; one big vortex in the vertical portion as in the cases with equal arm length and the second vortex above the first one. In the second case, (L_2/H_2 = 0.4), the vortex strength is a little less compared to the first case. The isotherms are more densely packed near the hot wall corner for L_2/H_2 = 0.65 than for L_2/H_2 = 0.4. This increases the heat transfer coefficient in the former case.

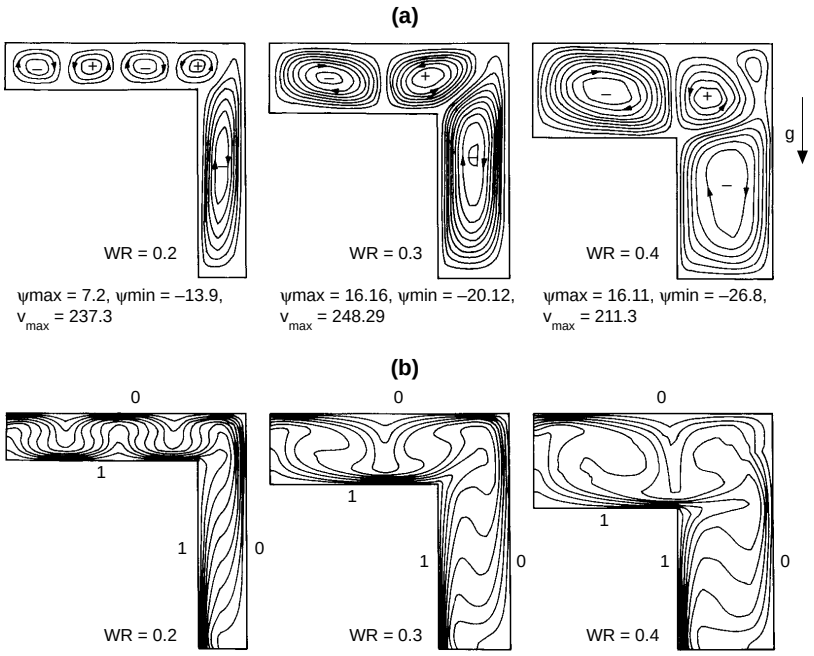

Figure 4.
Stream line (a) and isothermal (b) patterns for Ra = 10^6

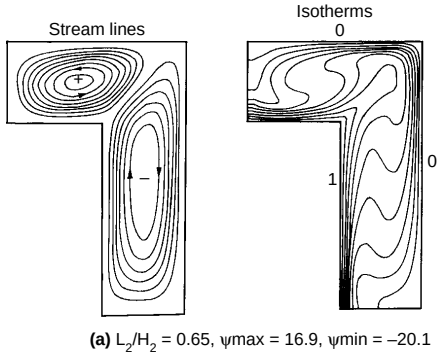

(a) L_2/H_2 = 0.65, ψmax = 16.9, ψmin = –20.1

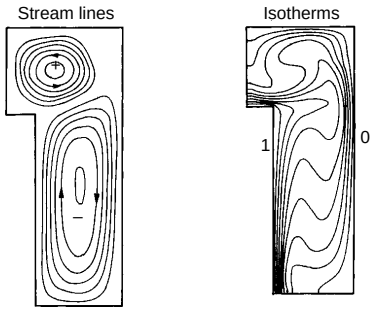

(b) L_2/H_2 = 0.4, ψmax = 12.84, ψmin = –18.23

Figure 5.
Stream line (a) and isothermal (b) patterns for Ra = 10^6 at different L_2/H_2 ratios

Nusselt number variation

The local Nusselt number is calculated as Nu = $\partial T/\partial n$ and the average Nusselt number is obtained by integrating the derivative over the wall length.

The local Nusselt number variation along the hot wall is shown in Figure 6 for different Rayleigh numbers and width ratios. It is seen that at low Rayleigh numbers a sharp peak in the Nusselt number value occurs at the vertex of the hot wall where the isotherms cluster near the corner (Figure 2). Also at low Rayleigh numbers the Nusselt number is inversely proportional to the width of the annulus as expected for the conduction dominated regime. At higher Rayleigh numbers, owing to convection effects, fluctuations in Nu value are observed indicating alternate spots of high and low heat flux. These fluctuations are consistent with the cellular pattern observed for the situation considered.

In Figures 7 and 8 the local Nusselt number variation along the hot wall is compared against the corresponding Nu variations for vertical and horizontal rectangular cavities respectively. In Figure 7 it is seen that the Nu variation for the odd-shaped cavity is quite similar to that for a vertical enclosure, especially at higher Rayleigh numbers. At low Rayleigh numbers the Nusselt number variation differs considerably from that for a vertical enclosure only around the sharp corner. From Figure 8 it is seen that the peak values of Nu for the

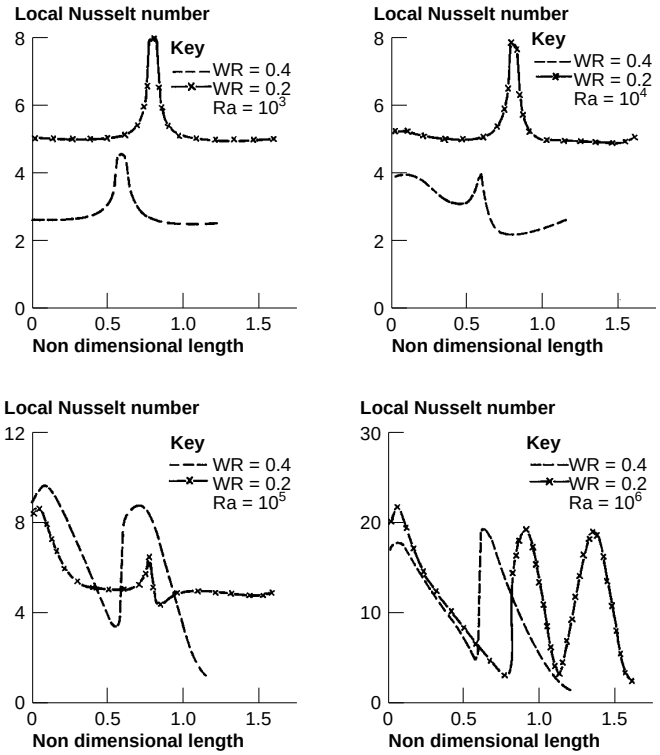

Figure 6.
Local Nusselt number variation along the hot wall at different Rayleigh numbers

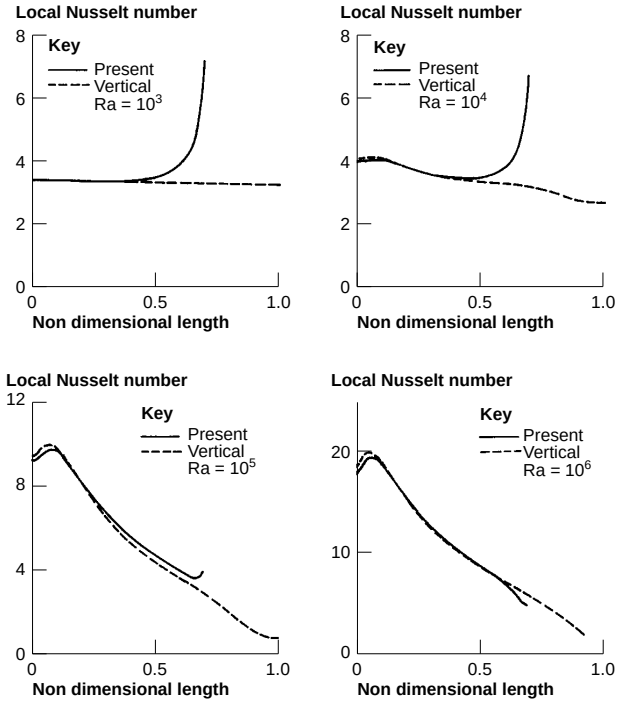

Figure 7.
Comparison of local Nusselt number along the hot vertical wall for the present geometry and a vertical cavity at different Rayleigh numbers

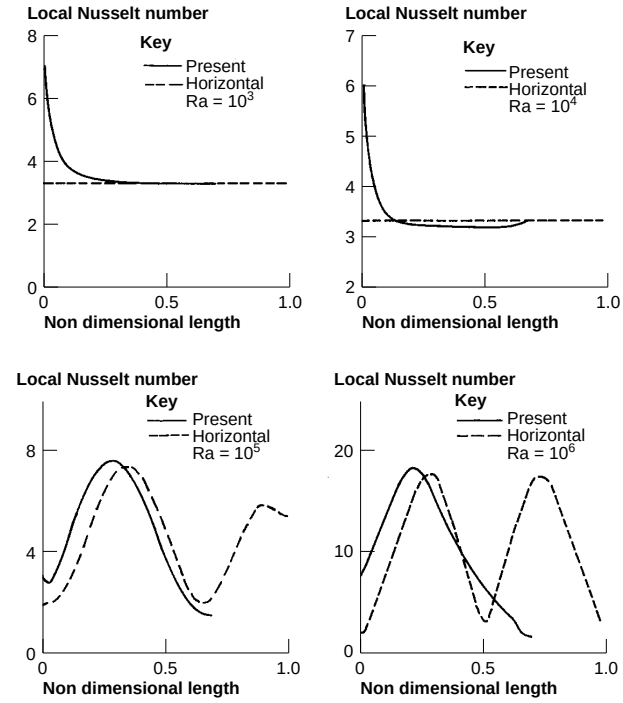

Figure 8.
Comparison of local Nusselt number along the hot horizontal wall for the present geometry and a horizontal cavity at different Rayleigh numbers

odd-shaped and horizontal enclosures are of the same order at high Rayleigh numbers. Moreover, the small shift in the location of peak Nu value is related to the shift in the locations of cellular vortices inside the horizontal portion, in the case of the odd-shaped geometry. This shift appears to be caused by penetration of vertical flow vortex into the horizontal chamber. At low Rayleigh numbers, the Nu variations are very similar except near the sharp corner. It can thus be argued that the flow and isothermal solutions for a complex geometry may be approximated in terms of vertical and horizontal sub-domains, with the sub-domains being selected appropriately. Such a procedure could be very useful for analysing the flow through complex passages in applications such as the cooling of electronic equipment. This feature is illustrated in Table IV, showing the average Nusselt number calculated for rectangular cavities of vertical/horizontal orientations and sub-domains of L-shaped cavity with similar orientations.

Average Nusselt number variation for different L_2/H_2 ratios are presented in Table V. The Nusselt number values are generally higher for the L-shaped cavity compared to those of the rectangular cavity. For L_2/H_2 values lower than unity, the Nusselt number in general increases.

Transient results

The transient variations of maximum Nu along both the walls and maximum velocity component values within the cavity are shown in Figure 9. For the hot wall the Nu is infinitely large initially owing to sudden imposition of the high temperature boundary condition; on the other hand, Nu starts from zero for the cold wall since T_c and T_i are equal. From the initial values, the Nusselt number decreases for the hot wall and increases for the cold wall until constant values

SI number	Ra	Vertical portion of the L-shaped cavity	Vertical cavity	Horizontal portion of the L-shaped cavity	Horizontal cavity
1	10^3	3.55	3.34	3.51	3.33
2	10^4	3.76	3.56	3.52	3.34
3	10^5	6.62	6.27	4.80	4.44
4	10^6	12.31	12.33	10.55	10.72

Table IV. Comparison of average Nusselt number values for vertical and horizontal sub-domains and rectangular cavities

SI number	Ra	$L_2/H_2 = 1$	$L_2/H_2 = 0.65$	$L_2/H_2 = 0.4$	Rectangular AR = 1.33
1	10^3	3.58	3.76	3.80	3.33
2	10^4	3.59	3.80	3.87	3.38
3	10^5	5.63	6.01	6.05	4.93
4	10^6	11.37	12.34	11.78	9.69

Table V. Comparison of average Nusselt number values for different L_2/H_2 ratios

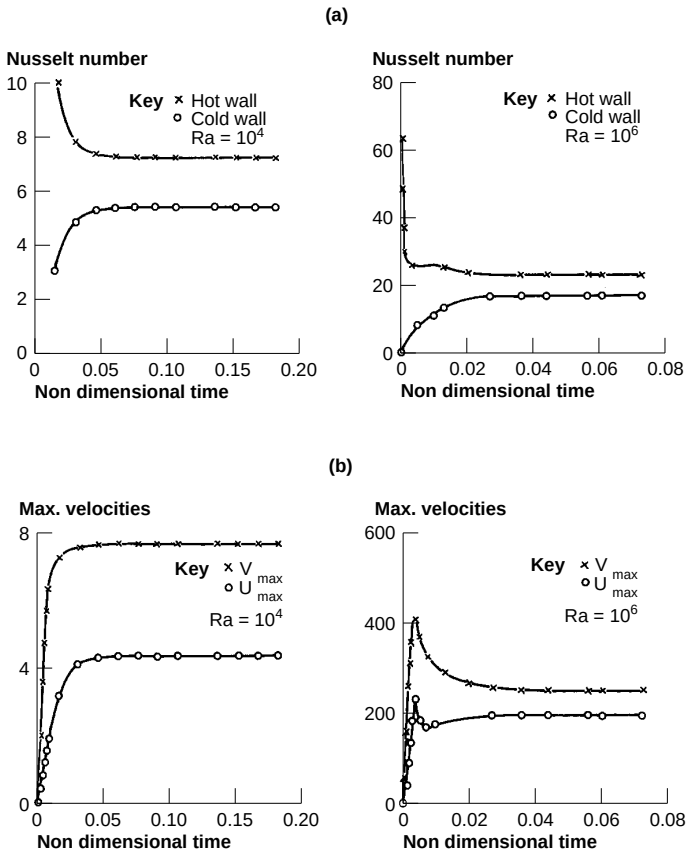

Figure 9.
(a) average Nusselt number variation with respect to time along the hot and cold walls at different Rayleigh numbers; (b) maximum vertical and horizontal velocities with respect to time at different Rayleigh numbers

are reached at steady state. At steady state, the average Nusselt number on the hot wall is higher than that of the cold wall because of the smaller surface area of the hot wall. At higher Rayleigh numbers, the initial transients in Nusselt number variation are much faster owing to higher velocity values encountered adjacent to the wall (see Figure 9). As regards the dimensionless velocities, their magnitudes are small at low Ra and high at higher Rayleigh numbers, as expected. For high Ra it is observed that an initial peak is reached which is greater than the steady state maximum value. The reason for this is that after the sudden imposition of the hot wall temperature the velocity in the vicinity of this wall shoots up rapidly owing to the occurrence of a thin convective layer. For later times, as convection effects penetrate throughout the cavity, the maximum velocity drops to a lower value.

Effects of boundary conditions

In order to investigate the effects of prescribed boundary conditions on the flow pattern and heat transfer phenomena, the prescribed temperature and adiabatic wall boundary conditions have been modified as discussed in the section

"Problem definition and formulation" and the results are presented in Figure 10. It is seen that a single vortex fills the entire space in this situation, except near the corners where small recirculating eddies with opposite sense of rotation are present. The isothermal patterns for this case are also quite different from those of the earlier problem studied.

If Figure 11, 12, 13, the flow and heat transfer phenomena are depicted at a higher Rayleigh number (Ra = 10^6) for the problem with modified interchanged conditions. In these figures it is observed that the natural convective flow does not reach steady state: rather, it has an oscillatory behaviour with counter rotating vortices originating periodically at the hot wall (bottom), which drift

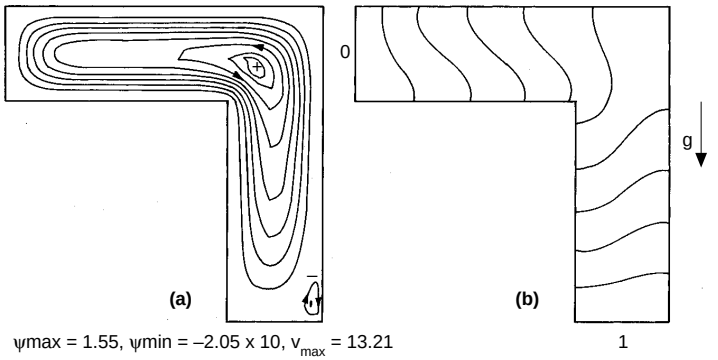

ψmax = 1.55, ψmin = –2.05 x 10, v_{max} = 13.21

Figure 10.
Flow (a) and isothermal (b) patterns for interchanged boundary conditions at Ra = 10^5 and WR = 0.3

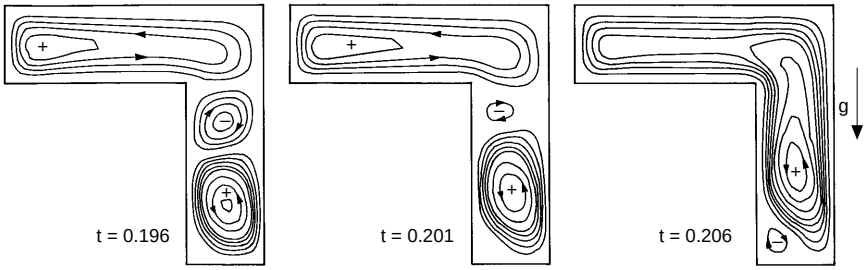

ψmax = 11.33, ψmin = –4.51, v_{max} = 135.4

ψmax = 10.86, ψmin = –1.34, v_{max} = 128.17

ψmax = 12.42, ψmin = –1.61, v_{max} = 140.24

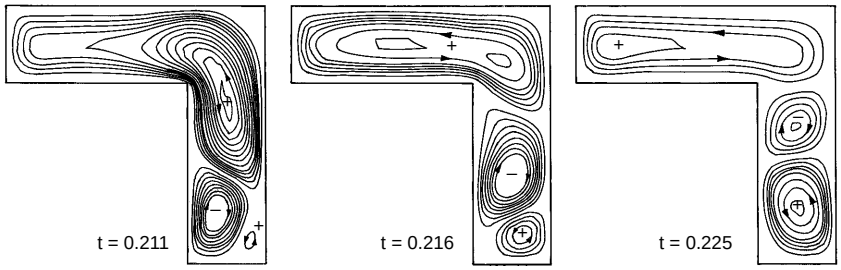

ψmax = 21.65, ψmin = –10.53, v_{max} = 256.8

ψmax = 9.4, ψ = –10.66, v_{max} = 122.48

ψmax = 11.55, ψmin = –5.0, v_{max} = 136.49

Figure 11.
Transient stream line patterns for interchanged boundary conditions at Ra = 10^6 and WR = 0.3

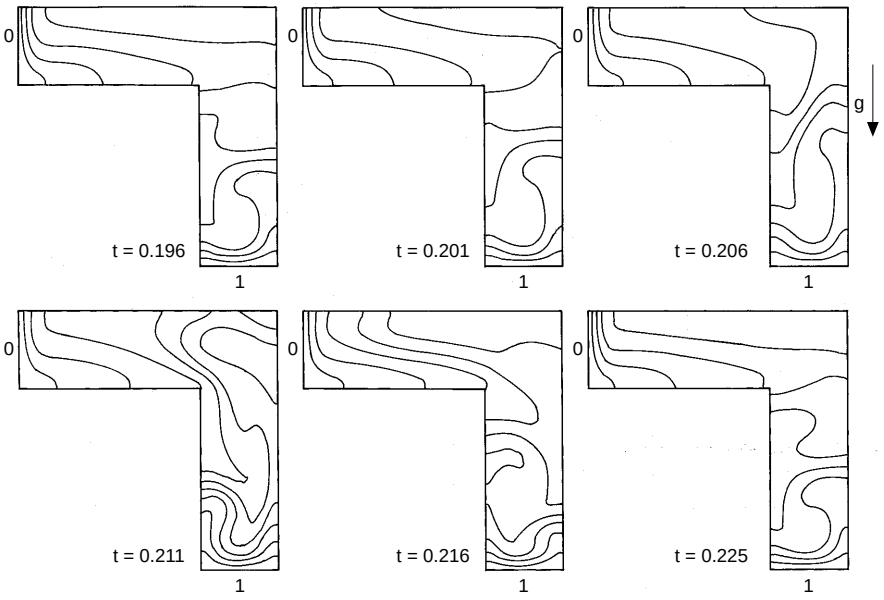

Figure 12.
Transient isothermal patterns for interchanged boundary conditions at Ra = 10^6 and WR = 0.3

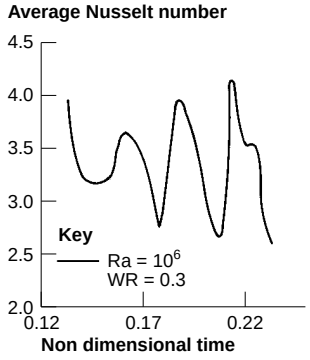

Figure 13.
Transient average Nusselt number variation at Ra = 10^6 and WR = 0.3

upwards and merge with the vortex of the horizontal portion. The corresponding isotherms (Figure 12) also indicate a cyclic variation with respect to time. The average Nusselt number along the hot wall also fluctuates periodically with time (Figure 13). These figures indicate that a steady state solution may not even exist for certain types of boundary conditions, for the geometry considered in the problem.

In Figure 14 a circular shaped hot inner body has been considered with the same boundary conditions as in Figure 1, at a Rayleigh number of 10^5. In this case it is seen that the vertical vortex is more predominant than the situation with rectangular inner body. The isothermal pattern is also quite different. This figure shows that the horizontal and vertical sub-domain approach discussed earlier could be applied only for regions where the inner and outer surfaces are parallel to each other.

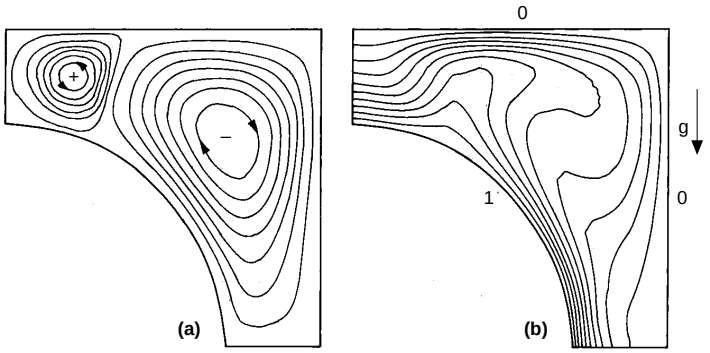

Figure 14.
Flow (a) and isothermal (b) patterns for a circular inner body

Conclusions

This study illustrates that a complex annular space with parallel opposite walls could be broken into several horizontal or vertical enclosures for the purpose of natural convective heat transfer analysis. It is also established that the nature of heat transfer changes with width ratio and Rayleigh number, for certain types of boundary conditions, steady states do not exist and oscillatory flow conditions are seen to prevail.

References

Aung, W. (Ed.) (1991), *Cooling Techniques for Computers*, Hemisphere Publishing Corporation, pp. 27, 166.

Betts, C., Boorman, C. and Sheriff, N. (1983), "Thermal striping in liquid cooled fast breeder reactors", *Proc. 2nd Int. Topical Meeting on Nuclear Reactor Thermal Hydraulics*, ANS, pp. 1292-1301.

Coulter, J.P. and Guceri, S.I. (1987), "Laminar turbulent natural convection within irregularly shaped enclosures", *Numerical Heat Transfer*, Vol. 12, pp. 211-27.

de Vahl Davis, G. (1983), "Natural convection of air in a square cavity: a bench mark numerical solution", *Int. J. Num. Meth. Fluids*, Vol. 3, pp. 249-64.

del Campo, E.M., Sen, M. and Ramos, E. (1988), "Analysis of laminar natural convection in triangular enclosure", *Numerical Heat Transfer*, Vol. 13, pp. 353-72.

Elder, J.W. (1965), "Laminar free convection in a vertical slot", *J. Fluid Mech.*, Vol. 23, pp. 77-98.

Evren-Selamet, E., Arpaci, V.S. and Borgnakke, C. (1992), "Simulation of laminar buoyancy driven flows in an enclosure", *Numerical Heat Transfer*, Part A, Vol. 22, pp. 401-20.

Fu, W. and Jou, Y. (1991), "A transient natural convection in a annular enclosure", *Int. Comm. Heat Mass Transfer*, Vol. 18, pp. 373-84.

Fu, W., Perng, J. and Shieh, W. (1989), "Transient laminar natural convection in an enclosure partitioned by an adiabatic baffle", *Numerical Heat Transfer*, Part A, Vol. 16, pp. 325-50.

Garg, V.K. (1992), "Natural convection between concentric spheres", *Int. J. Heat Mass Transfer*, Vol. 35, pp. 1935-46.

Glakpe, E.K. and Asfaw, A. (1991), "Prediction of two-dimensional natural convection in enclosures with inner bodies of arbitrary shapes", *Numerical Heat Transfer*, Part A, Vol. 20, pp. 279-96.

Nithiarasu, P., Seetharamu, K.N. and Sundararajan, T. (1995), "Natural convection in enclosures", *Proc. of second ISHMT and ASME conference and 13th National Heat and Mass Transfer Conference*, KREC, Surathkal, India.

Ostrach, S. (1988), "Natural convection in enclosures", *ASME J. Heat Transfer*, Vol. 110, pp. 1175-90.

Ramaswamy, B. (1988), "Finite element solution for advection and natural convection flows", *Computers & Fluids*, Vol. 16, pp. 349-88.

Ramaswamy, B., Jue, T.C. and Akin, J.E. (1992), "Semi-implicit and explicit finite element schemes for coupled fluid/thermal problems", *Int. J. Num. Meth. Engg*, Vol. 34, pp. 675-96.

Satya Sai, B.V.K., Seetharamu, K.N. and Aswatha Narayana, P.A. (1993), "Finite element analysis of effect of radius ratio on natural convection in an annular cavity", *Int. J. Num. Meth. Heat Fluid Flow*, Vol. 3, pp. 305-18.

Scozia, R. and Frederick, R.L. (1991), "Natural convection in slender cavities with multiple fine attached to an active wall", *Numerical Heat Transfer*, Part A, Vol. 20, pp. 127-58.

Tabarrok, B. and Lin, R.C. (1977), "Finite element analysis of free convection flows", *Int. J. Heat Mass Transfer*, Vol. 20, pp. 945-52.

Vafai, K. and Ettefagh, J. (1990), "The effects of sharp corners on buoyancy driven flows with particular emphasis on outer boundaries", *Int. J. Heat Mass Transfer*, Vol. 33, pp. 2311-28.

Warrington, R.O. and Powe, R.E. (1985), "The transfer of heat by natural convection between bodies and their enclosures", *Int. J. Heat Mass Transfer*, Vol. 28, pp. 319-30.

Yeung, W. (1989), "Analysis of natural convection in a closed vertical annulus", *Int. Comm. Heat Mass Transfer*, Vol. 16, pp. 445-55.

Yin, S.H., Wung, T.Y. and Chen, K. (1978), "Natural convection in an air layer enclosed within rectangular cavities", *Int. J. Heat Mass Transfer*, Vol. 21, pp. 307-15.